



An investigation on viscoelastic characteristics of 3D-printed FDM components using RVE numerical analysis

M. S. Anoop¹ · P. Senthil¹ · V. S. Sooraj²

Received: 25 May 2020 / Accepted: 9 November 2020 / Published online: 3 January 2021
© The Brazilian Society of Mechanical Sciences and Engineering 2021

Abstract

Fused deposition modelling (FDM) has emerged as an economical additive manufacturing method having the potential to fabricate functional components. Dynamic behaviour of FDM components is of great interest while designing and printing them for functional applications. This paper presents a methodology to describe the dynamic characteristics of FDM, combining the features of thermoplastic material and build parameters adopted in fabrication. The viscoelastic characteristics of thermoplastic filament induce time–temperature dependence in FDM components. The viscoelastic characteristic of the polymer is determined by dynamical mechanical analysis. Layer height is a significant build parameter that determines void geometry even in 100% infill printing, that influences mechanical properties of these additive manufactured components. Dynamic response of FDM 3D-printed parts is highly dependent on viscoelastic characteristics of polymer filaments and build parameters associated with printing. In the study, micro-scale models representing the features of actual cross section morphology with different layer heights are identified as representative volume element (RVE) models. Harmonic analysis is conducted on the RVE models using polymer material data approximated with generalized Maxwell model to determine the dynamic characteristics of the FDM print. The numerical analysis reveals orthotropic viscoelastic nature with maximum stiffness along the direction of filament deposition (raster) direction followed by transverse and vertical directions. A drastic reduction in the FDM component stiffness was observed at lower straining rates. The characteristics determined on RVE can be homogenized to the entire structure based on its print conditions and can be used for designing functional components.

Keywords Fused deposition modelling (FDM) · Representative volume element (RVE) · Homogenization · Viscoelastic · Dynamic mechanical analysis (DMA)

1 Introduction

Fused deposition modelling (FDM) has gained wide acceptance as most facile extrusion-based additive manufacturing technique. With reduced time from conceptual design to practical component, FDM has turned up as the most cost-effective additive manufacturing technique. The FDM components can be fabricated when and where it is needed

using simple fabrication set-up. The FDM components can be used for different applications such as structural, medical and electronic instrumentation components subjected to varying temperatures and dynamic conditions [1]. The thermoplastic polymers such as Polylactic acid (PLA), Poly-methyl methacrylate (PMMA), Polycarbonate (PC), Poly-phenyl-sulphone (PPSF), Polypropylene (PP), Polyethylene (PE), Polyamide (PA), Thermoplastic Polyurethane (TPU) and Acrylonitrile butadiene styrene (ABS) are most common thermoplastic polymer used for FDM fabrication. Further, Polyether ether ketone (PEEK) and Polyetherimide (PEI/ ULTEM) exhibit high thermal resistance and find interesting end use in high-temperature applications [2, 3]. With the usability of composite filaments in FDM, multifunctional components are developed in the form of capacitors [4], sensors [5, 6] and electronic instrumentation devices [7, 8].

The mechanical characteristics of FDM printed components are determined by the thermoplastic filament

Technical Editor: Aurelio Araujo.

✉ P. Senthil
senthil@nitt.edu

¹ Department of Production Engineering, National Institute of Technology, Tiruchirappalli, India

² Department of Aerospace Engineering, Indian Institute of Space Science and Technology, Thiruvananthapuram, India

material used for printing [9]. These thermoplastic polymers having viscoelastic characteristics induce time–temperature-dependent behaviour in FDM parts. However, as this manufacturing process relies on the fused deposition of filaments (raster), the rigidity of components is also persistent to the extent of fusion between adjacent rasters. The various parameters such as extrusion temperature, infill percentage, build orientation, raster width, feed rate, layer height, number of contours and build orientation affect the mechanical characteristics of the component. The dependence of raster angle on FDM strength was studied analytically, and its influence in part strength was experimentally validated [10]. The effect on number of contours was studied and developed an analytic model predicting the stiffness and ultimate strength, was developed for FDM parts processed with ABS [11]. Considering high strength required applications with 100% infill dense components, layer height and build orientation are influential in determining the mechanical characteristics [12]. The percentage of overlap between adjacent rasters governs the size of the voids at the interface. The extent of bonding is also influenced by the entanglement of melt across the interface. Such disentanglement effect on welding of rasters was studied analytically [13]. The mechanical characteristics of the FDM prints based on process parameters were experimentally analysed, and the print speed was found to have more impact on tensile strength [14].

The classical lamination theory (CLT) is useful to characterize the mechanical behaviour of 3D-printed parts. The yield criteria of CLT and Tsai Hill effectively predicted the in-plane strength, flexural strength and rigidity of FDM components [9, 15–17]. This approach is inadequate in addressing the effect of printing parameters such as degree of raster overlap, feed rate and nozzle temperature. The micro-scale features such as size and shape of void depend on the deposition criteria adopted in fabrication. The component was reported to exhibit anisotropic characteristics with maximum strength along axial direction followed by transverse and interlayer directions [18]. The mechanical characteristics of the printed components were effectively calculated through a multi-scale approach, capturing features of its cross-sectional morphology [19, 20]. The material properties derived from the finite element analysis (FEA) of representative volume element (RVE) can be homogenized to the entire component. This principle of numerical homogenization was substantiated with the strength of materials approach [21]. The studies based on numerical analyses of the approximated RVE model assumed symmetric voids between all the raster interfaces. The actual cross section-based void geometry of the component can be identified and numerically analysed to estimate the mechanical characteristics [22].

FDM fabrication involves the fused deposition of thermoplastic polymers having viscoelastic characteristics. Viscoelastic materials exhibit varying stress–strain characteristics based on the loading conditions. So, while designing FDM components, its time–temperature dependence needs to be considered. The thermoplastic materials exhibit varying stiffness with temperature change in glass transition. The factors influencing the glass transition temperature of epoxy materials used in civil structures were studied [23] and concluded that the factors such as post-curing, accelerated procedure, maximum temperature and heating rate influence the glass transition temperature value. FDM specimens in PLA and ABS with infill patterns were studied for its viscoelastic characteristics using dynamic mechanical analysis (DMA). The study revealed an increase in glass transition temperature with increase in frequency for FDM prints with different layer heights [24].

The multi-scale numerical procedure is commonly adopted in estimating the viscoelastic characteristics of composite structures. The transversely isotropic viscoelastic material characteristics of carbon fibre-reinforced plastic (CFRP) in the frequency domain were studied by numerical analysis [25]. Micro-scale numerical analysis was done on a statistically representative volume element to achieve the master curve for the complex constitutive model in the frequency domain. The master curve fitting was done by two approaches of generalised Maxwell model (GMM) and generalised fractional Maxwell model (GFMM). The predictions of numerical simulations were compared with Mori–Tanaka and Lielens analytical methods [26]. Polyvinyl Butyral, a commonly used interlayer material in laminate composites, was studied to determine viscoelastic characteristics using numerical analysis [27]. The experimental DMA results were used to extract viscoelastic characteristic and modified for an extended range of dynamic conditions. The master curves were obtained by using William–Landel–Ferry (WLF) expression, and Prony series based on GMM was fitted to the experimental data for numerical analysis. The temperature dependence of TPU was studied using DMA, and an artificial neural network (ANN) model was presented to predict the dynamic mechanical behaviour [28]. The dynamic mechanical characteristics of inkjet prints using Objet Connex printer were studied for different test configurations, print directions and on materials used [29]. Among test configurations of tensile and bending modes, tensile mode reported higher storage modulus and loss factor peak values. The inkjet printer materials exhibited wide variations in storage modulus.

Researchers are focusing towards the development of FDM components having applications in different fields of medical, automotive, aerospace and instrumentation. FDM components find a better lightweight replacement for

automotive and aerospace parts as acoustic liners, inlet guide vanes, engine access doors and rover parts [30]. The functional components in such aerospace application may experience dynamic load in a wide range of frequency and varying temperature, affecting the part quality [31], necessitates the investigation on viscoelastic characteristics of FDM components.

The prime focus of the current research is to study the time–temperature-dependent viscoelastic characteristics of the FDM components. In this study, a multi-scaled numerical homogenization technique is portrayed for determining the viscoelastic characteristics of FDM components. This research also aims to study the viscoelastic effect of FDM components with different layer heights. PLA is selected as the filament material for the study as it is commonly used biocompatible FDM material. Experimental DMA is done to determine the viscoelastic nature of the print material with different frequencies of 0.1, 1, 5 and 10 Hz for the temperature range of 35 to 80 °C. These DMA results are then utilized to generate a master curve for a broader range of frequency using the WLF shift factor. The master curve data is approximated with GMM using Prony series constants. Then, virtual DMA on RVE models capturing the print characteristics for different layer heights of 0.1, 0.2, 0.3 and 0.4 mm is simulated to study the effect of layer height. Harmonic analysis on the RVE models with six independent periodic boundary conditions are applied to determine the directional characteristics in the frequency range of 1×10^{-3} to 1×10^3 Hz. The dynamic characteristics are estimated by numerical DMA and homogenized over the entire region of the component. The proposed solution projects viscoelastic behaviour as a function of frequency and print parameters.

2 Investigations on viscoelastic behaviour in FDM

2.1 Viscoelastic formulation

When viscoelastic material subjected to an oscillating harmonic strain, the material develops stress response in harmonic with the applied strain, which lags by an angle called phase lag (δ). The harmonic strain applied and stress responses are shown in Eqs. 1 and 2. The ratio of stress response to the strain applied in the dynamic condition is called dynamic modulus or complex modulus (E^*). Due to the phase lag of the stress response, the dynamic modulus has two components[32]. The component in phase with the applied strain is called storage modulus (E'), and the out phase component is loss modulus (E'') as shown in Eqs. 3–5.

$$\varepsilon = \varepsilon_0 e^{i\omega t} \quad (1)$$

$$\sigma = \sigma_0 e^{i(\omega t - \delta)}, \quad (2)$$

where ε and σ are the harmonic strain applied and stress response; ε_0 and σ_0 are the amplitude of the harmonic strain applied and stress response; ω is circular frequency and δ is phase lag.

$$E^* = E' + iE'' = \frac{\sigma_0 e^{-i\delta}}{\varepsilon_0} = \frac{\sigma_0 \cos(\delta)}{\varepsilon_0} - i \frac{\sigma_0 \sin(\delta)}{\varepsilon_0} \quad (3)$$

$$E' = \frac{\sigma_0 \cos(\delta)}{\varepsilon_0} \quad (4)$$

$$E'' = \frac{\sigma_0 \sin(\delta)}{\varepsilon_0}, \quad (5)$$

where the ratio of loss modulus to the storage modulus is called loss factor denoted by $\tan(\delta)$ as shown in Eq. 6.

$$\tan(\delta) = \frac{E''}{E'}. \quad (6)$$

2.2 Modelling of viscoelasticity

The viscoelastic characteristics can be mathematically modelled as a combination of linear elastic and viscous elements. Among the models, Maxwell and Kelvin models are the two-element model with elastic and viscous element combinations. In the Maxwell model, the two elements are considered in series combination where as in Kelvin model the elements are in parallel combination. There are three-element and four-element combinations in the Burgers model for representing various viscoelastic performances. Such models may not be accurately representing the behaviour of many viscoelastic materials. The viscoelastic characteristic can be more accurately captured by increasing the number of elastic and damping elements. Generalized Maxwell model (GMM) and generalized Kelvin model (GKM) are models representing a number of elastic and viscous elements in combination. In GMM, several Maxwell elements are connected in parallel, whereas in GKM, several Kelvin elements connected in series. Straining GMM causes prescribed straining on individual Maxwell elements (comprising elastic and viscous elements in series), causes resultant stress as the cumulative sum of the individual contributions. Among these models, GMM is more capable of predicting viscoelastic characteristic of materials with the strain history data [33, 34]. The GMM with a number of Maxwell elements can be applied as material characteristic data for numerical analysis using Prony series coefficients of relaxation time (τ) and weights (α). The Prony series coefficients

represent GMM viscoelastic characteristics of the material for the numerical harmonic analysis [32, 35].

$$E'(\omega) = E_0 \left[1 - \sum_{i=1}^N \alpha_i \right] + E_0 \sum_{i=1}^N \frac{\tau_i^2 \alpha_i \omega^2}{1 + \tau_i^2 \omega^2} \quad (7)$$

$$E''(\omega) = E_0 \sum_{i=1}^N \frac{\tau_i \alpha_i \omega}{1 + \tau_i^2 \omega^2}, \quad (8)$$

where E' , E'' are storage and loss modulus, E_0 is the time-independent elastic modulus of the material, τ and α are the relaxation time and weights of Prony series constants applied in GMM and N is the number of Maxwell elements used in Prony series representation.

2.3 Dynamic mechanical analysis

The viscoelastic properties such as storage and loss modulus of specimen material can be determined by dynamic mechanical analysis (DMA). The effect of test configurations and types of equipment on DMA results was studied for different modes like simply cantilever, double cantilever and three-point bending were analysed using three different analysers. The results showed that each DMA analyser has its formulation for determining complex modulus resulting in some discrepancies even if the test conditions are the same. The three-point bending test mode was found to be least affected by the geometry and test parameters as clamping effects are avoided [36].

To study the viscoelastic characteristics of the polymer, DMA was done on FDM specimen fabricated using PLA filament in three-point bending mode. The specimens were fabricated with a least possible layer height of 0.06 mm to avoid the effect of voids. DMA was performed using 'Perkin Elmer DMA 8000' analyser following ASTM D4065 standard [37]. All the specimen were fabricated using 'Ultimaker 3 Extended' using PLA filament of 2.85 mm diameter procured from 'WOL 3D'. The FDM specimens of rectangular cross section were prepared with a thickness of 3 mm, breadth 12 mm and length of 60 mm, in 0/90 degree raster orientation with 100% infill density. The specimens were analysed for varying temperature from 35 to 80 °C at a rate of 5 °C per minute; at frequencies of 0.1, 1, 5 and 10 Hz.

2.4 Numerical viscoelasticity analysis

The experimentally determined viscoelastic characteristics of the polymer for a shorter range of frequencies are extended to a broader range of frequency or time by applying the time-temperature superposition (TTS) principle. TTS is achieved by WLF shift factor as given in Eq. 9. With the

shift factor, the DMA results can be extended to plot the master curve for a wider range of frequencies or time[38].

$$\log a_t = \frac{-C_1(T - T_g)}{C_2 + (T - T_g)}, \quad (9)$$

where $\log a_t$ is the shift factor in logarithmic form, T is the temperature of selected data set for shifting, with glass transition temperature (T_g) considered as reference temperature, the constants C_1 and C_2 are approximated to 17.44 and 51.6, respectively.

The glass transition temperature of the polymer is obtained by differential scanning calorimetry (DSC) analysis. The analysis was performed on PLA filament specimen using 'Pyris 6 DSC 6000'. The temperature range of 30 to 250 °C at a rate of 5 °C per minute was adopted for the test.

The master curve for the viscoelastic behaviour is approximated using Generalized Maxwell Model (GMM) storage and damping attributes, as shown in Eqs. 7 and 8. The GMM model with a number of Maxwell elements using Prony series coefficients of relaxation time (τ) and weights (α) fits the experimental data.

2.5 Micro-scale RVE model based on cross-sectional morphology

Even in 100% infill dense FDM samples, voids are generated on the interface of adjacent rasters. The print parameter controls extend of overlap between rasters and thereby shape and size of voids at the interface. The geometry of these voids influences the mechanical characteristics of FDM prints. The cross section morphology of FDM samples with 100% infill density was examined to determine the geometry of voids. FDM samples were printed with PLA filament with 2.85 mm diameter procured from 'WOL 3D' for different layer heights of 0.1, 0.2, 0.3 and 0.4 mm with the parameters as depicted in Table 1. The specimens were then sectioned, and the cross section surfaces were sputtered, and scanning electron microscopy (SEM) images were captured using 'VEGA3 TESCAN'. The SEM of the sectioned surface

Table 1 FDM print parameters adopted for cross section morphology analysis

| Print parameter | Values |
|------------------------------|--------------------|
| Layer height (mm) | 0.1, 0.2, 0.3, 0.4 |
| Raster width (mm) | 0.44 |
| Infill line distance (mm) | 0.4 |
| Nozzle diameter (mm) | 0.4 |
| Printing temperature (°C) | 190 |
| Build plate temperature (°C) | 50 |
| Print speed (mm/s) | 60 |

displayed a regular array of voids. The void geometry is used for estimating the micro-scale RVE geometry capturing features of the FDM component. Using ‘ANSYS Space Claim Direct Modeler’, the three-dimensional models with recurring features apprehending the geometry of voids were created.

2.6 Viscoelastic constitutive model

The properties of FDM prints depend upon the thermoplastic material used for fused deposition and the build parameters adopted for printing. FDM components exhibit orthotropic viscoelastic characteristics with the complex constitutive model given in Eq. 10. The dynamic behaviour of the RVE is estimated in harmonic numerical analysis by applying six independent harmonic oscillatory strains and periodic boundary conditions.

$$\begin{bmatrix} \bar{\sigma}_{11} \\ \bar{\sigma}_{22} \\ \bar{\sigma}_{33} \\ \bar{\sigma}_{12} \\ \bar{\sigma}_{13} \\ \bar{\sigma}_{23} \end{bmatrix}_{(\omega)} = \begin{bmatrix} \bar{C}_{11}^* & \bar{C}_{12}^* & \bar{C}_{13}^* & 0 & 0 & 0 \\ \bar{C}_{12}^* & \bar{C}_{22}^* & \bar{C}_{23}^* & 0 & 0 & 0 \\ \bar{C}_{13}^* & \bar{C}_{23}^* & \bar{C}_{33}^* & 0 & 0 & 0 \\ 0 & 0 & 0 & \bar{C}_{44}^* & 0 & 0 \\ 0 & 0 & 0 & 0 & \bar{C}_{55}^* & 0 \\ 0 & 0 & 0 & 0 & 0 & \bar{C}_{66}^* \end{bmatrix} \begin{bmatrix} \bar{\epsilon}_{11} \\ \bar{\epsilon}_{22} \\ \bar{\epsilon}_{33} \\ \bar{\gamma}_{12} \\ \bar{\gamma}_{13} \\ \bar{\gamma}_{23} \end{bmatrix}_{(\omega)}, \quad (10)$$

where $\{\bar{\sigma}_{ij}\}_{(\omega)}$ and $\{\bar{\epsilon}_{ij}, \bar{\gamma}_{ij}\}_{(\omega)}$ are volume average stress and strain tensor computed at frequency ‘ ω ’ over the volume of RVE and $C^*_{ij(\omega)}$ are the elements of the complex constitutive matrix at that frequency.

$$\bar{C}^*_{ij(\omega)} = \frac{\text{Volume average of elemental stress in RVE}}{\text{Corresponding strain applied to RVE}}, \quad \text{i.e. } \bar{C}^*_{ij(\omega)} = \frac{\bar{\sigma}_{ij(\omega)}}{\epsilon_{ij(\omega)}}. \quad (11)$$

Considering phase lag in different frequencies of dynamic loading, the constitutive element for storage modulus and loss modulus can be expressed as Eqs. 12 and 13.

$$\bar{C}'_{ij} = \frac{\bar{\sigma}_{ij(\omega)}}{\epsilon_{ij(\omega)}} \cos(\delta_{(\omega)}) \quad (12)$$

$$\bar{C}''_{ij} = \frac{\bar{\sigma}_{ij(\omega)}}{\epsilon_{ij(\omega)}} \sin(\delta_{(\omega)}), \quad (13)$$

where $\bar{\sigma}_{ij} = \frac{1}{V_{RVE}} \int \sigma_{ij} dv$ and $\delta_{(\omega)}$ is the phase lag depending on the loading frequency.

The numerical analysis was done in FEA software ‘ANSYS Workbench’ using harmonic response analysis systems. The dynamic characteristics obtained from the DMA of polymer were used to simulate the harmonic responses on micro-scale FDM RVE model with viscoelastic material properties using GMM with Prony series constants as described in Sect. 2.3. The Prony series coefficients assigned

as PLA material for the numerical analysis are depicted in Table 2. For determining the directional viscoelastic characteristics, RVE model was subjected to six independent harmonic strains with frequencies ranging from 1×10^{-3} to 1×10^3 Hz. The six harmonic strains include three normal strains and three shear strains with maximum amplitudes of 1% deformation. The RVE model was applied with six independent harmonic oscillatory strains with periodic boundary conditions as depicted in Table 3. The elemental stress developed in the model was extracted, and volume averages were estimated with script command using ‘ANSYS APDL’. The volume averages of elemental stress were evaluated for ten different frequencies with the range of the harmonic analysis. The in-phase and out phase components of volume average stress response were estimated using the phase angle of different frequencies in the range of the analysis. The constitutive elements for the RVE model were estimated separately for stiffness and damping components using Eqs. 10 to 13. The viscoelastic constants were estimated from the compliance matrix corresponding to the constitutive model. The RVE’s complex characteristics can be homogenized for the entire structure of the FDM prints.

2.7 Experimental validation

The literature pointed out that, the viscoelastic characteristic effect can be simulated by the application of varying straining rate to features the dynamic effects on the specimen [39]. The orthotropic viscoelastic characteristics can

be validated with tensile testing at the different straining rates [40]. The virtual numerical DMA was experimentally validated by conducting tensile testing at the different rates of straining. The tensile test was conducted by following ASTM D 638. The FDM test specimens were fabricated with 0.4 mm layer height by adopting the print parameters

Table 2 Prony series coefficients for PLA

| Relaxation times (τ_i) | Weights (α_i) |
|-------------------------------|------------------------|
| 0.280251548 | 0.019244785 |
| 8.400548668 | 0.287630107 |
| 0.353635827 | 0.114373691 |
| 0.924534243 | 0.072134943 |
| 0.947203477 | 0.130956286 |
| 0.953961166 | 0.281296897 |
| 0.095833253 | 0.047115016 |
| 0.019792124 | 0.019505246 |

Table 3 Displacement boundary constrains for RVE with dimensions a, b and c (as shown in Fig. 4c) for six independent harmonic deformation

| Harmonic strain amplitude | Harmonic displacement amplitude constrains along direction (mm) | | |
|---------------------------|---|---|---|
| | 1 (Raster direction) | 2 (Transverse direction) | 3 (Vertical direction) |
| $\epsilon_{11} = 0.01$ | $u_{1(0,y,z)} = 0,$ $u_{1(a,y,z)} = a \times 0.01$ | $u_{2(x,0,z)} = 0,$ $u_{2(x,b,z)} = 0$ | $u_{3(x,y,0)} = 0,$ $u_{3(x,y,c)} = 0$ |
| $\epsilon_{22} = 0.01$ | $u_{1(0,y,z)} = 0,$ $u_{1(a,y,z)} = 0$ | $u_{2(x,0,z)} = 0,$ $u_{2(x,b,z)} = b \times 0.01$ | $u_{3(x,y,0)} = 0,$ $u_{3(x,y,c)} = 0$ |
| $\epsilon_{33} = 0.01$ | $u_{1(0,y,z)} = 0,$ $u_{1(a,y,z)} = 0$ | $u_{2(x,0,z)} = 0,$ $u_{2(x,b,z)} = 0$ | $u_{3(x,y,0)} = 0,$ $u_{3(x,y,c)} = c \times 0.01$ |
| $\gamma_{12} = 0.01$ | $u_{1(0,y,z)} = 0,$ $u_{1(a,y,z)} = b \times 0.05$ | $u_{2(x,0,z)} = 0,$ $u_{2(x,b,z)} = a \times 0.05$ | $u_{3(x,y,0)} = 0,$ $u_{3(x,y,c)} = 0$ |
| $\gamma_{13} = 0.01$ | $u_{1(0,y,z)} = 0,$ $u_{1(a,y,z)} = c \times 0.05$ | $u_{2(x,0,z)} = 0,$ $u_{2(x,b,z)} = 0$ | $u_{3(x,y,0)} = 0,$ $u_{3(x,y,c)} = a \times 0.05$ |
| $\gamma_{23} = 0.01$ | $u_{1(0,y,z)} = 0,$ $u_{1(a,y,z)} = 0$ | $u_{2(x,0,z)} = 0,$ $u_{2(x,b,z)} = c \times 0.05$ | $u_{3(x,y,0)} = 0,$ $u_{3(x,y,c)} = b \times 0.05$ |

depicted in Table 1. The ASTM 638 specimen was modelled using 'ANSYS Space Claim Direct Modeler' and then processed using slicing software 'Ultimaker Cura 3.2' for the imparting the print parameters and build orientations (along axis 1, 2 and 3). The tensile specimens were fabricated in 'Ultimaker 3.2' with the print parameters in three different print orientations as along the raster, transverse and vertical directions. The specimen printed with loading along axis 1 (raster direction) exhibited the characteristics of E1. Similarly, the specimen printed along axis 2 (transverse direction) and axis 3 (vertical direction) were tested for obtaining the elastic modulus along with those directions (E2 and E3). The tensile tests were conducted on 'Tinius Olsen H25KL' at different crosshead speeds of 0.048, 0.48, 2.4 and 4.8 mm per minute. The crosshead speeds are selected corresponding to dynamic effect due to the harmonic analysis frequencies of 0.1, 1, 5 and 10 Hz with an amplitude of 1% deformation. Twelve tensile samples were printed in each orientation for conducting the tensile test with three specimens each at the four different rates of straining.

3 Results and discussion

3.1 Viscoelastic characterization of PLA based on experimental DMA

The storage modulus and loss modulus data obtained from the DMA are shown in Fig. 1. At lower temperature, the PLA specimen exhibited higher stiffness with storage modulus above 3000 MPa in all set of analysis. As the temperature rises, experiments showed a swift reduction in storage modulus in the vicinity of the glass transition temperature.

The PLA specimen exhibited a reduction of storage modulus by 90% with an increase in temperature beyond its glass transition. The reduction of storage modulus was observed with a synchronized increment of loss modulus in all the dynamic analysis. Loss factor also showed variation with experimentation frequency. With the increase in experimentation frequency, the temperature corresponding to the peak of loss factor also increased. The temperature at the peak of loss factor denotes the glass transition temperature. The glass transition of the specimen was observed at different temperatures with respect to the experimentation frequencies. At glass transition temperature of the component, viscous behaviour becomes active with a reduction in stiffness due to the dissipation of energy by deforming the component structure. The experiment with 0.1 Hz frequency exhibited the lower glass transition temperature, whereas, with the increase in experiment frequency, the higher transition temperature was reported. With a higher frequency of loading, the energy gets stored in the component and behaves stiffer, whereas the lower rate of loading allows the material to dissipate more energy by deforming.

The experimental data results were utilized to generate a master curve for a broader range of frequency using the WLF shift factor. The master curve for extended frequency range was established using glass transition temperature determined from DSC analysis as reference temperature for TTS. The glass transition temperature of PLA filament was found to be 64.4 °C, as shown in Fig. 2. The master curve obtained was approximated using GMM with eight terms Prony series coefficients. The Prony series coefficients were procured by minimizing the error function of nonlinear least-square fit using solver function in Microsoft Excel depicted in Table 2. The GMM-approximated SM and LM, and the experimental results with TTS are shown in Fig. 3a, b.

Fig. 1 DMA results for PLA

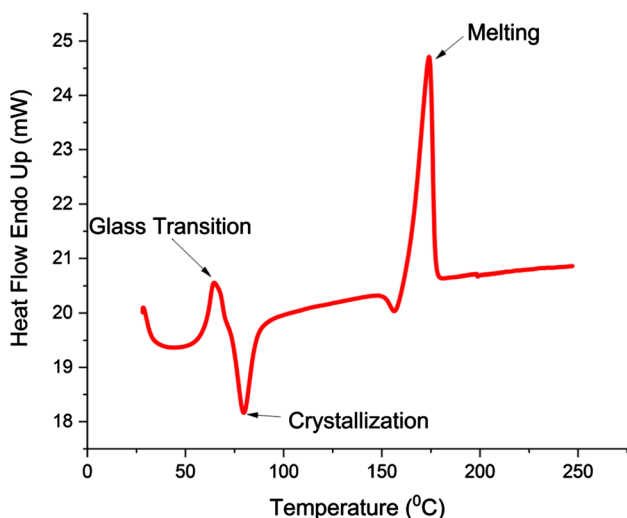
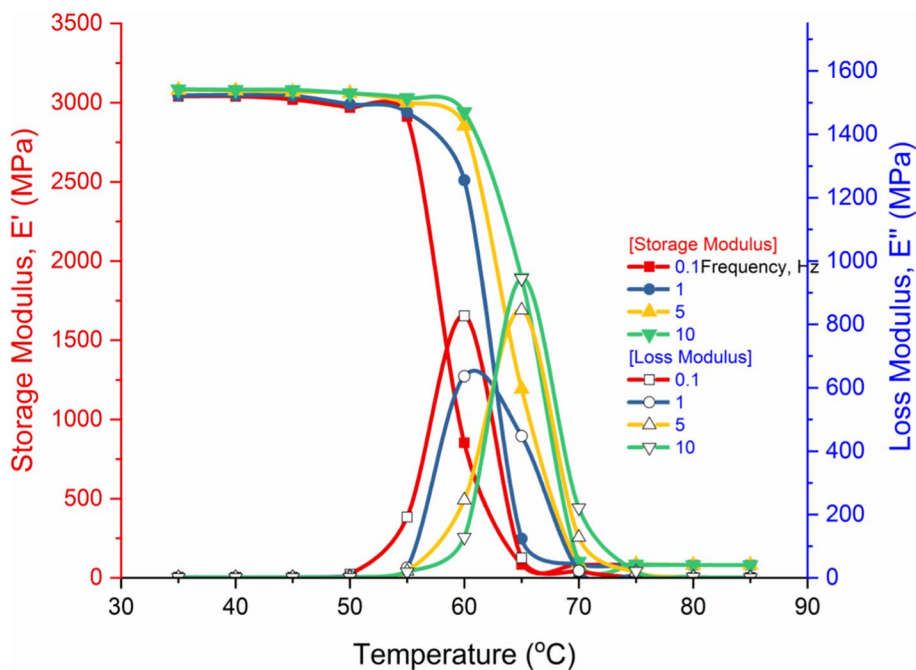


Fig. 2 DSC analysis results for PLA

3.2 Discussion on RVE and numerical modelling outcomes

3.2.1 Micro-scale RVE model

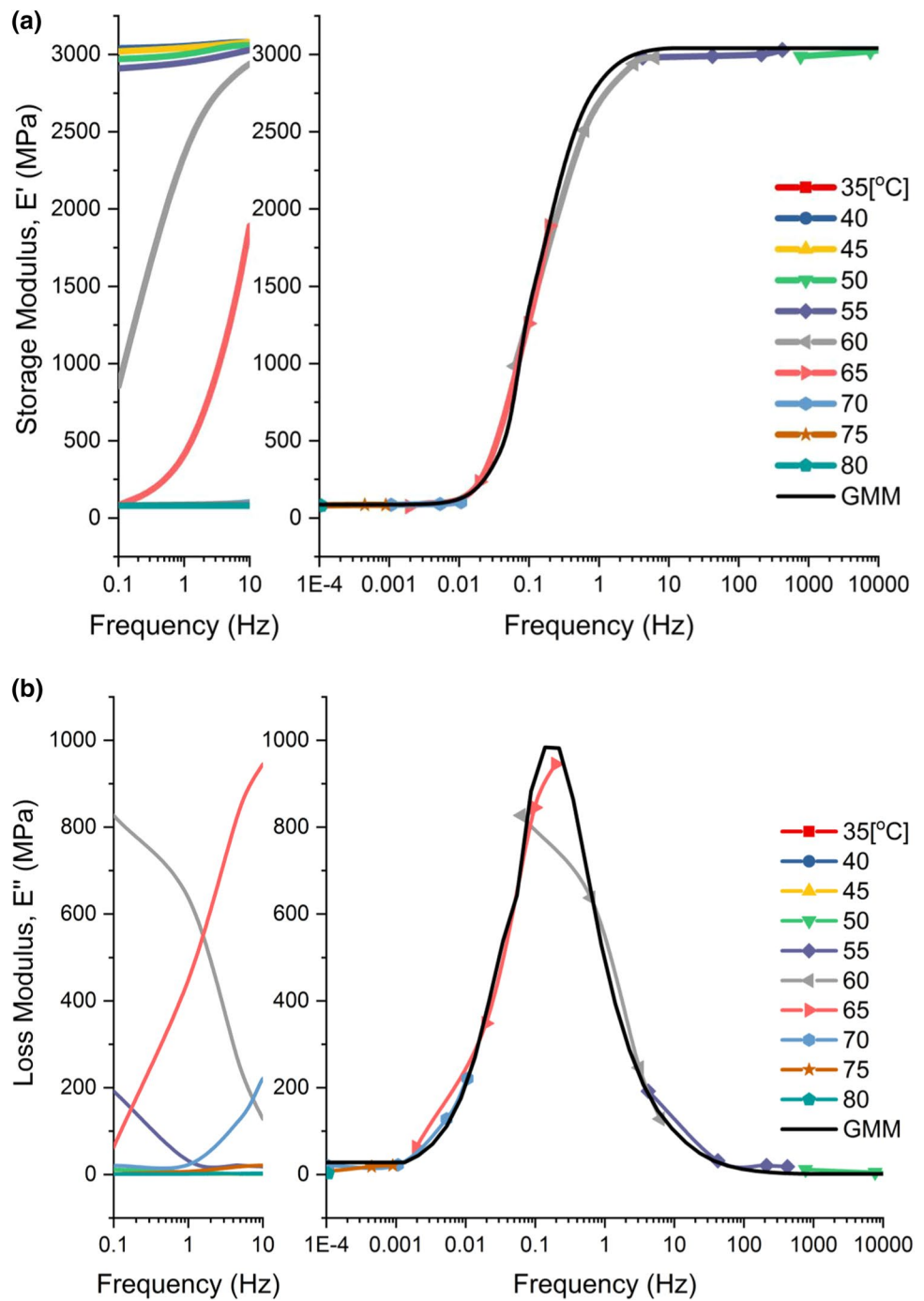
The dependence of print parameters on FDM components is due to the extent of fusion between the rasters. The extent of

coalescence between rasters was observed from the cross-sectional morphology of the component. The SEM image of the cross section revealed the presence of a regular array of voids in the component [22]. This regular array of voids imparts the orthotropic characteristics to the component. The geometric form of voids for different layer heights was analysed; the void geometry was in the form of a triangle with a flat base along with the interface of layers and curved lateral surface due to the adherence of adjacent rasters along with a layer as shown in Fig. 4a. Periodic micro-scale unit cells are identified as RVE which is shown in Fig. 4b. Figure 4c represents the RVE modelled based on the actual cross-sectional morphology of the FDM part.

3.2.2 Numerical investigation and validation of dynamic characteristics of FDM components

The harmonic responses of the RVE models subjected to six independent harmonic strains were used for estimating the directional viscoelastic characteristics. With the viscoelastic nature of the filament material, the stress response lags the applied strain with a phase angle. For experimental validation, the numerical results of 0.4 mm layer height are compared with the tensile test results conducted at four crosshead speeds of 0.048, 0.48, 2.4 and 4.8 mm per minute on ASTM 638 samples of 0.4 mm

Fig. 3 The GMM-approximated **a** storage modulus with the experimental results and **b** loss modulus with the experimental results



layer height. The test was repeated with three samples in each straining rate in the three orientations to determine the mean elastic constants. The mean value of experimental elastic modulus in the three orientations at each straining rate was considered for comparing with

numerical harmonic analysis in corresponding frequencies. The experimentation with different crosshead speeds showed different stiffness. The specimen with a lower rate of straining exhibited lowest mean elasticity modulus of 1012.5 MPa in specimen printed along the vertical

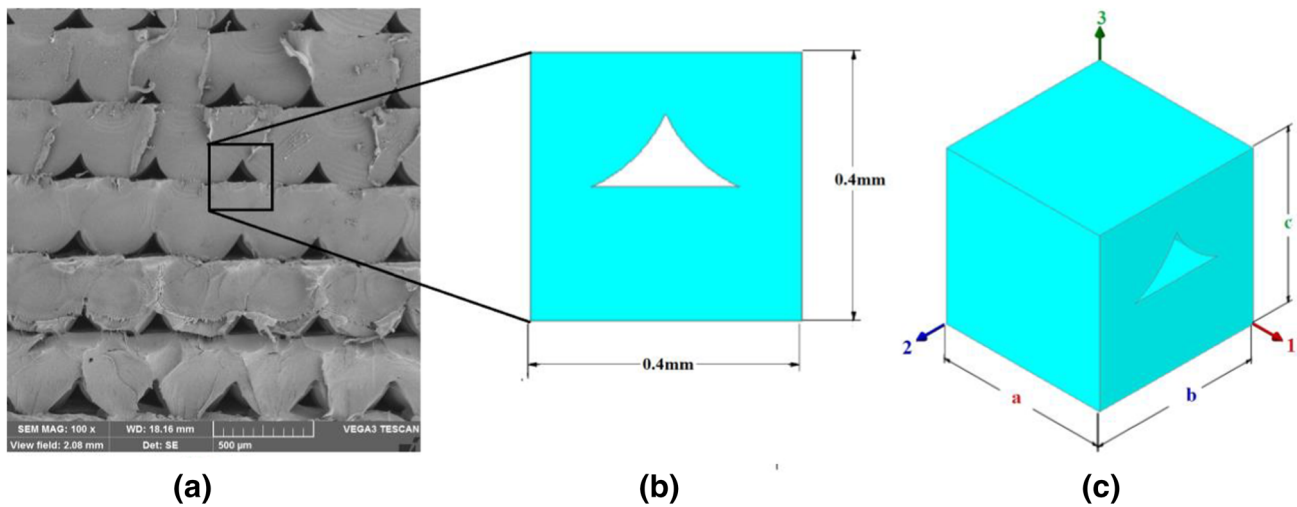


Fig. 4 The RVE modelled based on the actual cross-sectional morphology of the print. **a** Actual cross section morphology, **b** repetitive array of rasters with void and **c** RVE model

direction. The specimen with the loading axis along the raster direction was reported maximum mean elastic modulus of 3192.84 MPa. Experimentation results endorsed the numerical analysis with a steep variation in elastic modulus with the rate of straining of samples in all the print orientations. Lower values of mean elastic modulus were exhibited at lower straining rates, and it increased with an increase in the rate of straining. The numerical results with the corresponding frequency were comparable with the experimental test with a maximum deviation of 8.39% obtained in case of vertically printed samples. The comparison of experimental results with numerical results is shown in Table 4.

From the numerical DMA, it was observed that the storage modulus drastically reduces to about 8% of the maximum stiffness at lower straining frequencies. It was observed with an increase in loss modulus. With lower frequency, the polymer molecules achieve more mobility, and thereby the component deforms easier, resulting in the lower magnitude of the elemental stress response. Due to this, the strain energy is dissipated by the deformation of the component and exhibits more viscous characteristics. At higher frequency, the straining energy is stored in the components and results in higher elemental stress response with increase in the stiffness of the component, exhibiting elastic characteristics.

The geometry of the RVE also influences the storage and loss modulus. The dynamic response of the FDM

components shows the directional variation with respect to the layer height adopted in its fabrication. At a higher frequency of straining, models with the lower layer height exhibit higher stiffness compared to that with higher layer heights. The RVE model, with a layer height of 0.4 mm, reported a reduction of storage modulus by 34% at a lower frequency of loading. The model exhibited predominant elastic characteristics for frequencies beyond 10 Hz. The maximum storage modulus along the in-plane transverse direction (along axis 2) was observed 10% less than that in raster direction at higher straining frequencies. Similarly, a reduction of 28% of the storage modulus was observed in vertical (along axis 3) direction. The RVE model with higher layer height models exhibits higher loss modulus representing the damping behaviour. The characteristic curves of numerical DMA for different conditions of straining are shown in Fig. 5a–f. The cross section morphology revealed an increase in void size with the layer height. The FDM prints with 0.1 mm layer height exhibited almost isotropic viscoelastic characteristics. The rasters bounded with larger voids have less resistance to deformation; thereby, straining energy is dissipated in deformation. The material discontinuity due to the geometry of void in vertical direction provides more feasibility for material deformation than in transverse direction. This causes a reduction of stiffness in the vertical and transverse directions. The complex moduli for FDM samples at different harmonic frequencies are depicted in Table 5.

Table 4 Comparison of the present study with tensile test results

| Tensile test_ Straining rate (Numerical analysis_ Fre- quency) | E ₁ (MPa) | | | E ₂ (MPa) | | | E ₃ (MPa) | | |
|--|----------------------|------------------|-------------|----------------------|------------------|-------------|----------------------|------------------|-------------|
| | Present study | Tensile test | Deviation % | Present study | Tensile test | Deviation % | Present study | Tensile test | Deviation % |
| | Mean ± SD | | | Mean ± SD | | | Mean ± SD | | |
| 0.048 mm/min (0.1 Hz) | 1106.49 | 1197.55 ± 176.27 | 7.60 | 1074.92 | 1115.25 ± 174.28 | 3.75 | 973.76 | 1012.5 ± 194.13 | 3.83 |
| 0.48 mm/min (1 Hz) | 2554.89 | 2785.35 ± 163.13 | 8.27 | 2295.37 | 2354.5 ± 197.52 | 2.58 | 1850.44 | 1707.25 ± 210.15 | - 8.39 |
| 2.4 mm/min (5 Hz) | 3012.73 | 2871.28 ± 210.13 | - 4.93 | 2701.78 | 2583.30 ± 168.45 | - 4.38 | 2168.83 | 2035.15 ± 187.33 | - 6.57 |
| 4.8 mm/min (10 Hz) | 3037.62 | 3192.84 ± 210.13 | 4.86 | 2723.89 | 2772.35 ± 168.45 | 1.78 | 2186.12 | 2110.5 ± 187.33 | - 3.58 |

The component stiffness along the raster direction reported maximum stiffness, and that along transverse and vertical direction reported a reduction in storage modulus of 10% and 28%, respectively.

The higher strain rate of FDM components indicates higher stiffness, while the decline in strain rate results in lower component stiffness. The higher straining rate restricts material mobility to a higher extend. This causes the storage of energy within the component without much deformation and rapidly restores to equilibrium. Lower straining rate permits relatively more material mobility and thereby dissipates energy for deformation. The viscoelastic characteristics, as determined from the numerical analysis, can be used by designers for designing applications subjected to dynamic loading. The directional properties of the FDM components, along with its viscoelastic characteristics, need to be analysed for determining the complex mechanical behaviour.

4 Conclusion

The viscoelastic properties obtained from the numerical analysis of micro-scale RVE can be homogenized for the FDM parts fabricated with same parameters. The RVE-based homogenized properties provide the befitting material data for numerical simulations of the functional FDM components. The thermoplastic material used in FDM brings out the viscoelastic attributes on the print, while the build parameter induces orthotropic nature to the FDM component. The primary focus of this work is to study the effect of the viscoelastic behaviour of the FDM components.

The dynamic characteristics of the polymer are determined from experimental DMA, and the results are extrapolated for a broader range of frequencies using the WLF equation. TTS data was GMM-approximated by Prony series constants for numerical analysis. Numerical DMA was simulated on micro-scale RVE representing the actual cross section of FDM prints with different layer heights. The numerical results of RVE with 0.4 mm layer height were validated with experimental testing.

The numerical dynamic analysis revealed the dependence of layer height and material characteristics in the FDM components. The layer height controls the void geometry and thereby influences the material mobility on straining the component. The build parameter of layer height also influences the directional viscoelastic characteristics in dynamic loading condition. Further, the orthotropic viscoelastic characteristics were more predominant with higher layer heights.

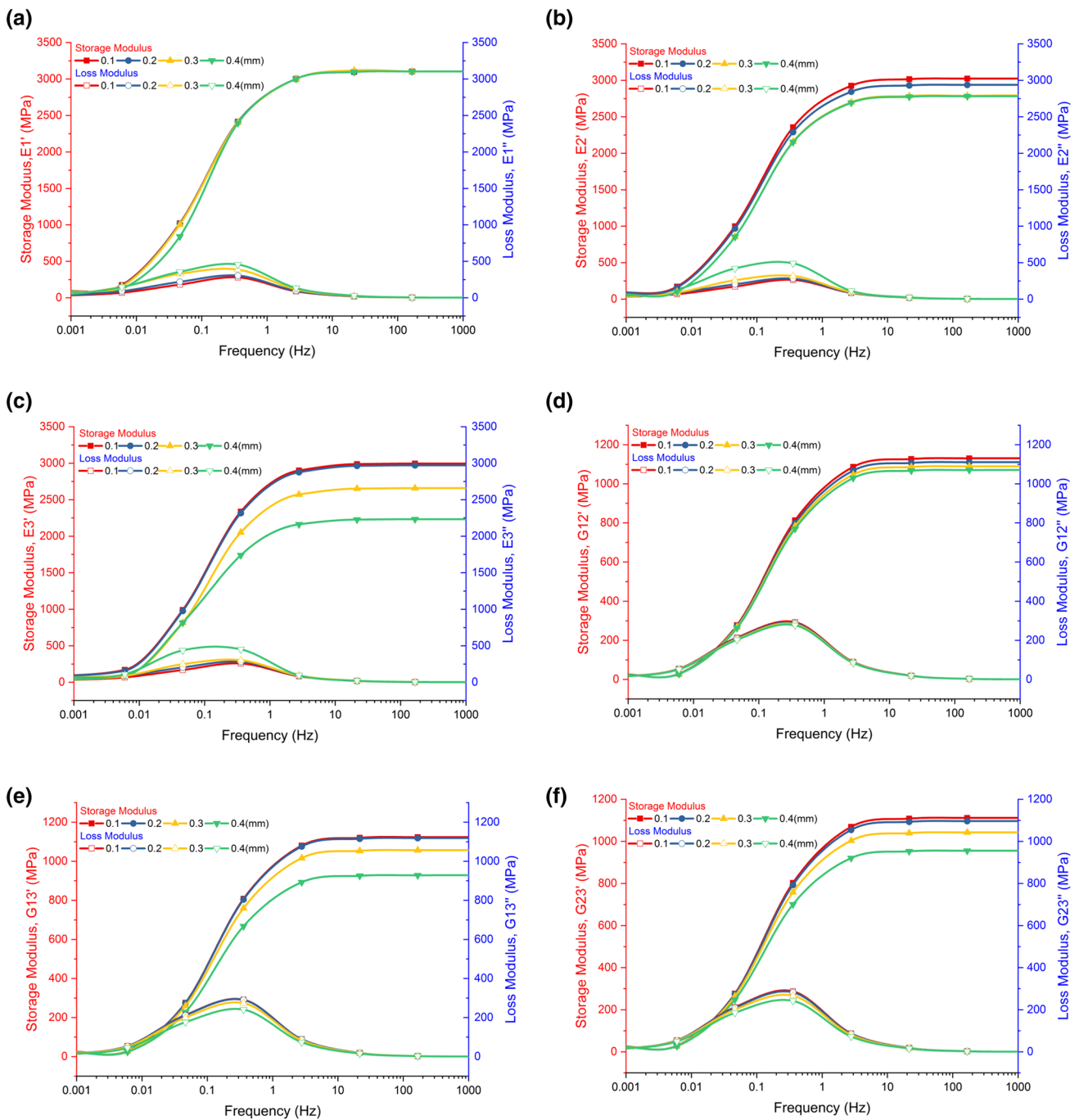


Fig. 5 The characteristic curves of numerical DMA for different conditions of straining **a** storage modulus and loss modulus along direction 1, **b** storage modulus and loss modulus along direction 2, **c** storage modulus and loss modulus along direction 3, **d** shear storage

modulus and loss modulus along plane 12, **e** shear storage modulus and loss modulus along plane 13, **f** shear storage modulus and loss modulus along plane 23

As researches are focusing on the applicability of functional FDM components in severe dynamic and thermal conditions, necessitates the determination of its dynamic characteristics. RVE-based numerical dynamic analysis is capable of determining the dynamic

mechanical characteristics of FDM prints. This technique can be further extended to study the thermal and electrical characteristics of FDM components printed using conductive polymer filaments.

Table 5 Complex modulus for FDM samples at different harmonic frequencies

| Frequency (Hz) | Layer height (mm) | Storage modulus, E' (MPa) | | | Loss modulus, E'' (MPa) | | | Loss factor, $\tan(\delta)$ | | |
|----------------|-------------------|-----------------------------|---------|---------|---------------------------|--------|--------|-----------------------------|------|------|
| | | Direction | | | | | | | | |
| | | 1 | 2 | 3 | 1 | 2 | 3 | 1 | 2 | 3 |
| 0.01 | 0.1 | 258.27 | 253.27 | 251.35 | 80.24 | 77.89 | 76.56 | 0.31 | 0.31 | 0.30 |
| | 0.2 | 249.12 | 238.30 | 240.83 | 102.92 | 97.55 | 98.14 | 0.41 | 0.41 | 0.41 |
| | 0.3 | 239.62 | 176.97 | 182.57 | 165.62 | 106.73 | 102.33 | 0.69 | 0.60 | 0.56 |
| | 0.4 | 192.29 | 175.92 | 169.69 | 166.48 | 161.19 | 141.71 | 0.87 | 0.97 | 0.84 |
| 0.1 | 0.1 | 1258.60 | 1230.89 | 1220.78 | 197.10 | 187.98 | 182.94 | 0.16 | 0.15 | 0.15 |
| | 0.2 | 1253.02 | 1193.56 | 1206.38 | 232.72 | 216.47 | 216.68 | 0.19 | 0.18 | 0.18 |
| | 0.3 | 1242.67 | 1076.75 | 1149.90 | 338.04 | 268.72 | 257.27 | 0.27 | 0.25 | 0.22 |
| | 0.4 | 1106.49 | 1074.92 | 1027.47 | 372.82 | 432.78 | 440.19 | 0.34 | 0.46 | 0.41 |
| 1 | 0.1 | 2570.04 | 2507.26 | 2484.93 | 228.45 | 216.69 | 210.43 | 0.09 | 0.09 | 0.08 |
| | 0.2 | 2568.40 | 2436.01 | 2463.45 | 249.06 | 229.53 | 229.49 | 0.10 | 0.09 | 0.09 |
| | 0.3 | 2561.41 | 2301.72 | 2189.47 | 314.83 | 258.78 | 247.40 | 0.12 | 0.11 | 0.11 |
| | 0.4 | 2554.89 | 2295.38 | 1850.45 | 370.45 | 390.83 | 357.38 | 0.14 | 0.14 | 0.15 |
| 10 | 0.1 | 3038.28 | 2961.07 | 2933.67 | 62.04 | 58.85 | 57.17 | 0.02 | 0.02 | 0.02 |
| | 0.2 | 3038.23 | 2876.69 | 2909.51 | 66.51 | 61.21 | 61.22 | 0.02 | 0.02 | 0.02 |
| | 0.3 | 3038.96 | 2732.51 | 2601.96 | 80.99 | 66.99 | 63.99 | 0.03 | 0.02 | 0.02 |
| | 0.4 | 3037.62 | 2723.89 | 2186.12 | 93.22 | 79.09 | 67.04 | 0.03 | 0.03 | 0.03 |
| 100 | 0.1 | 3099.16 | 3020.11 | 2992.14 | 10.20 | 9.67 | 9.40 | 0.00 | 0.00 | 0.00 |
| | 0.2 | 3099.13 | 2933.90 | 2967.40 | 10.90 | 10.03 | 10.04 | 0.00 | 0.00 | 0.00 |
| | 0.3 | 3099.55 | 2785.95 | 2654.84 | 13.20 | 10.93 | 10.44 | 0.00 | 0.00 | 0.00 |
| | 0.4 | 3099.15 | 2778.17 | 2228.89 | 15.14 | 12.83 | 10.87 | 0.00 | 0.00 | 0.00 |

Compliance with ethical standards

Conflict of interest The article titled 'An investigation on viscoelastic characteristics of 3D-printed FDM components using RVE numerical analysis' is our original research work and has not been submitted to, nor is under review at, another journal or other publishing venue. All authors included in the manuscript have contributed towards the conceptual design, analysis interpreting results and preparing the manuscript. Further, the authors declare that they have no known competing financial interests or personal relationships that could have appeared to influence the work reported in this paper.

References

- Mohan N, Senthil P, Vinodh S, Jayanth N (2017) A review on composite materials and process parameters optimisation for the fused deposition modelling process. *Virtual Phys Prototyp* 2759:47–59. <https://doi.org/10.1080/17452759.2016.1274490>
- Yang C, Wang B, Li D, Tian X (2017) Modelling and characterisation for the responsive performance of CF/PLA and CF/PEEK smart materials fabricated by 4D printing. *Virtual Phys Prototyp* 12:69–76. <https://doi.org/10.1080/17452759.2016.1265992>
- Miyase A, Qu S, Lo KH, Wang SS (2020) Elevated-temperature thermal expansion of PTFE/PEEK matrix composite with random-oriented short carbon fibers and graphite flakes. *J Eng Mater Technol* 142:1–10. <https://doi.org/10.1115/1.4045158>
- Isakov DV, Lei Q, Castles F, Stevens CJ, Grovenor CRM, Grant PS (2016) 3D printed anisotropic dielectric composite with meta-material features. *Mater Des* 93:423–430. <https://doi.org/10.1016/j.matdes.2015.12.176>
- Sathies T, Senthil P, Prakash C (2019) Application of 3D printed PLA-carbon black conductive polymer composite in solvent sensing. *Mater Res Express* 6:115349. <https://doi.org/10.1088/2053-1591/ab5040>
- Jayanth N, Senthil P (2019) Application of 3D printed ABS based conductive carbon black composite sensor in void fraction measurement. *Compos Part B* 159:224–230. <https://doi.org/10.1016/j.compositesb.2018.09.097>
- Schmitz DP, Ecco LG, Dul S, Pereira ECL, Soares BG, Barra GMO, Pegoretti A (2018) Electromagnetic interference shielding effectiveness of ABS carbon-based composites manufactured via fused deposition modelling. *Mater Today Commun* 15:70–80. <https://doi.org/10.1016/j.mtcomm.2018.02.034>
- Sathies T, Senthil P, Anoop MS (2020) A review on advancements in applications of fused deposition modelling process. *Rapid Prototyp J*. <https://doi.org/10.1108/RPJ-08-2018-0199>
- Somireddy M, Singh CV, Czekanski A (2020) Mechanical behaviour of 3D printed composite parts with short carbon fiber reinforcements. *Eng Fail Anal* 107:1–13. <https://doi.org/10.1016/j.engfailanal.2019.104232>
- Huang B, Singamneni S (2015) Raster angle mechanics in fused deposition modelling. *J Compos Mater* 49:363–383. <https://doi.org/10.1177/0021998313519153>
- Croccolo D, De Agostinis M, Olmi G (2013) Experimental characterization and analytical modelling of the mechanical behaviour of fused deposition processed parts made of ABS-M30. *Comput Mater Sci* 79:506–518. <https://doi.org/10.1016/j.commatsci.2013.06.041>

12. Dizon JRC, Espera AH Jr, Chen Q, Advincula RC (2018) Review mechanical characterization of 3D-printed polymers. *Addit. Manuf.* 2018:44–67. <https://doi.org/10.1016/j.addma.2017.12.002>
13. McIlroy C, Olmsted PD (2017) Disentanglement effects on welding behaviour of polymer melts during the fused-filament-fabrication method for additive manufacturing. *Polymer (Guildf)*. 123:376–391. <https://doi.org/10.1016/j.polymer.2017.06.051>
14. Abbott AC, Tandon GP, Bradford RL, Koerner H, Baur JW (2018) Process-structure-property effects on ABS bond strength in fused filament fabrication. *Addit Manuf* 19:29–38. <https://doi.org/10.1016/j.addma.2017.11.002>
15. Somireddy M, Czepakanski A (2020) Anisotropic material behavior of 3D printed composite structures: material extrusion additive manufacturing. *Mater Des.* <https://doi.org/10.1016/j.matdes.2020.108953>
16. Kumar Mishra SP (2020) Prediction of in-plane stiffness of multi-material 3D printed laminate parts fabricated by FDM process using CLT and its mechanical behaviour under tensile load. *Mater Today Commun* 45:50. <https://doi.org/10.1016/j.mtcomm.2020.100955>
17. Casavola C, Cazzato A, Moramarco V, Pappalettere C (2016) Orthotropic mechanical properties of fused deposition modelling parts described by classical laminate theory. *Mater Des* 90:453–458. <https://doi.org/10.1016/j.matdes.2015.11.009>
18. Roy Xu L, Leguillon D (2020) Dual-notch void model to explain the anisotropic strengths of 3D printed polymers. *J Eng Mater Technol* 142:3–6. <https://doi.org/10.1115/1.4044282>
19. Calneryte D, Barauskas R, Milasiene D, Maskeliunas R, Neciunas A, Ostreika A, Patasius M, Krisciunas A (2018) Multi-scale finite element modeling of 3D printed structures subjected to mechanical loads. *Rapid Prototyp J* 24:177–187. <https://doi.org/10.1108/RPJ-05-2016-0074>
20. Somireddy M, Czepakanski A (2017) Mechanical characterization of additively manufactured parts by FE modeling of mesostructure 1–21. <https://doi.org/10.3390/jmmp1020018>
21. Rodríguez JF, Thomas JP, Renaud JE (2003) Mechanical behavior of acrylonitrile butadiene styrene fused deposition materials modeling. *Rapid Prototyp J* 9:219–230. <https://doi.org/10.1108/13552540310489604>
22. Anoop MS, Senthil P (2019) Homogenisation of elastic properties in FDM components using microscale RVE numerical analysis. *J Braz Soc Mech Sci Eng.* <https://doi.org/10.1007/s40430-019-2037-8>
23. Michels J, Widmann R, Czaderski C, Allahvirdizadeh R, Motavalli M (2015) Glass transition evaluation of commercially available epoxy resins used for civil engineering applications. *Compos Part B Eng* 77:484–493. <https://doi.org/10.1016/j.compositesb.2015.03.053>
24. Selva Priya M, Naresh K, Jayaganthan R, Velmurugan R (2019) A comparative study between in-house 3D printed and injection molded ABS and PLA polymers for low-frequency applications. *Mater Res Express* 6:085345. <https://doi.org/10.1088/2053-1591/ab2776>
25. Liebig WV, Jackstadt A, Sessner V, Weidenmann KA, Kärger L (2019) Frequency domain modelling of transversely isotropic viscoelastic fibre-reinforced plastics. *Compos Sci Technol* 180:101–110. <https://doi.org/10.1016/j.compscitech.2019.04.019>
26. Pathan MV, Tagarielli VL, Patsias S (2017) Numerical predictions of the anisotropic viscoelastic response of uni-directional fibre composites. *Compos Part A Appl Sci Manuf* 93:18–32. <https://doi.org/10.1016/j.compositesa.2016.10.029>
27. Pelayo F, Lamela-Rey MJ, Muniz-Calvente M, López-Aenlle M, Álvarez-Vázquez A, Fernández-Canteli A (2017) Study of the time-temperature-dependent behaviour of PVB: application to laminated glass elements. *Thin Walled Struct* 119:324–331. <https://doi.org/10.1016/j.tws.2017.06.030>
28. Kopal I, Harničárová M, Valíček J, Kušnerová M (2017) Modeling the temperature dependence of dynamic mechanical properties and visco-elastic behavior of thermoplastic polyurethane using artificial neural network. *Polymers (Basel)*. <https://doi.org/10.3390/polym9100519>
29. Reichl KK, Inman DJ (2018) Dynamic mechanical and thermal analyses of objet connex 3D printed materials. *Exp Technol* 42:19–25. <https://doi.org/10.1007/s40799-017-0223-0>
30. Stratasys (2013) 3D Printing a space vehicle
31. Joshi SC, Sheikh AA (2015) 3D printing in aerospace and its long-term sustainability. *Virtual Phys Prototyp* 10:175–185. <https://doi.org/10.1080/17452759.2015.1111519>
32. Kaliske M, Rothert H (1997) Formulation and implementation of three-dimensional viscoelasticity at small and finite strains. *Comput Mech* 19:228–239. <https://doi.org/10.1007/s004660050171>
33. Findley WN, Lai JS, Onaran K (1976) Creep and relaxation of nonlinear viscoelastic materials with an introduction to linear viscoelasticity. [https://doi.org/10.1016/0032-3861\(78\)90187-8](https://doi.org/10.1016/0032-3861(78)90187-8)
34. Serban D-A (2016) Viscoplastic behaviour of polyamides. *Viscoelastic Viscoplastic Mater.* <https://doi.org/10.5772/64563>
35. ANSYS Workbench 19.0 User's Guide (2019) ANSYS Workbench 19.0 User's Guide, 4.7.3.1 Prony Series Complex Modulus
36. Henriques IR, Borges LA, Costa MF, Soares BG, Castello DA (2018) Comparisons of complex modulus provided by different DMA. *Polym Test* 72:394–406. <https://doi.org/10.1016/j.polymertesting.2018.10.034>
37. ASTM International (2012) ASTM D4065-Standard Practice for Plastics: Dynamic Mechanical Properties—Determination and Report of Procedures. <https://doi.org/10.1520/d4065-12.1.8>
38. Williams ML, Landel RF, Ferry JD (1955) The temperature dependence of relaxation mechanisms in amorphous polymers and other glass-forming liquids. *J Am Chem Soc* 77:3701–3707. <https://doi.org/10.1021/ja01619a008>
39. Bartolini L, Iannuzzi D, Mattei G (2018) Comparison of frequency and strain-rate domain mechanical characterization. *Sci Rep* 8:1–11. <https://doi.org/10.1038/s41598-018-31737-3>
40. Yan S, Deng J, Bae C, Kalnaus S, Xiao X (2020) Orthotropic viscoelastic modeling of polymeric battery separator. *J Electrochem Soc* 167:090530. <https://doi.org/10.1149/1945-7111/ab8a99>

Publisher's Note Springer Nature remains neutral with regard to jurisdictional claims in published maps and institutional affiliations.